Research Square

Preprints are preliminary reports that have not undergone peer review.
They should not be considered conclusive, used to inform clinical practice,
or referenced by the media as validated information.

Performance improvement of Cd-free CIGS Solar Cells Using ZnS Buffer Layers Prepared by Solvothermal Routes: Experimental and Device Simulation

Abdelhafid Mouhoub

a.mouhoub@lagh-univ.dz

Amar Telidji University of Laghouat

Wahiba Chatta

Amar Telidji University of Laghouat

Mouhoub Birane

Amar Telidji University of Laghouat

Research Article

Keywords: ZnS, buffer layer, Solvothermal, thin films, CIGS solar cells, SCAPS-1D

Posted Date: November 16th, 2026

DOI: https://doi.org/10.21203/rs.3.rs-11495025/v1

License: This work is licensed under a Creative Commons Attribution 4.0 International License.
Read Full License

Additional Declarations: No competing interests reported.

Performance improvement of Cd-free CIGS Solar Cells Using ZnS Buffer Layers Prepared by Solvothermal Routes: Experimental and Device Simulation

Abdelhafid Mouhoub[1,*], Wahiba Chatta[2], and Mouhoub Birane[3]

[1]Department of Electronics, Laboratory of Physical Chemistry of Materials, Amar Telidji University, B.P. 37G, 03000 Laghouat, Algeria

[2]Department of Electronics, Laboratory of Materials for the Application and Valorization of Renewable Energies, Amar Telidji University, B.P. 37G, 03000 Laghouat, Algeria

[3]Department of Electronics, Laboratory of Materials, Energy Systems, Renewable Energies and Energy Management (LMSEERGE), Amar Telidji University, B.P. 37G, 03000 Laghouat, Algeria

*Corresponding author: a.mouhoub@lagh-univ.dz

ABSTRACT

In this work, we investigate the synthesis and characterization of the ZnS layer as an alternative Cd-free buffer layer for $Cu(In,Ga)Se_2$ (CIGS) thin film solar cells, The ZnS nanopowders were successfully prepared via solvothermal method, then employed to fabricate thin films deposited by rf-magnetron sputtering. Their structural, morphological and optical characterizations were performed. In addition, these experimental data obtained were further implemented in numerical simulations of a p-CIGS/n-ZnS heterojunction using SCAPS-1D. The impact of different buffer layer materials CdS and ZnS on the performance of CIGS solar cells was thoroughly compared and analyzed. The obtained results demonstrate that, the films crystallize in the cubic phase with grain sizes ranging from 4 to 20 nm and exhibiting high transparency (> 90%), with a tunable band gap in the range of 3.68 to 3.8 eV. The tuning of the deposition conditions allows ZnS to achieve proper band alignment with the CIGS absorber. The optimized structure revealed that, both the buffer material and their thickness significantly influence the overall device performance. The substitution of the conventional CdS buffer with ZnS this possesses a wider bandgap, resulted in lower conversion efficiency due to unfavorable energy band alignment at the interface. To overcome this limitation and enhance short-wavelength absorption, a novel CdS/ZnS double buffer layer structure was proposed. The optimization of this configuration improved the cell efficiency from 22.62% to 24.68%. These results indicate the potential of ZnS-based buffers as promising and environmentally friendly alternatives for high efficiency CIGS solar cells.

Keywords: ZnS, buffer layer, Solvothermal, thin films, CIGS solar cells, SCAPS-1D.

1 Introduction

Thin film solar cells on $Cu(In,Ga)Se_2$ (CIGS) have attracted extensive consideration due to their high absorption coefficient, long carrier diffusion length [1, 2], and the ability to achieve power conversion efficiencies above 23% [3]. Despite their excellent performance, most high-efficiency CIGS devices still rely on CdS as the buffer layer, which raises environmental concerns associated to cadmium toxicity and leads to parasitic absorption losses appropriate to its compact bandgap (~2.4 eV) [4-6]. Therefore, the development of efficient and environmentally friendly Cd-free buffer layers has become a crucial research direction in advancing CIGS photovoltaic technologies [7].

Among the proposed alternatives, Zn-based chalcogenides such as ZnS have shown promising potential due to their wide and tunable bandgaps, excellent optical transparency, and favorable band alignment with the CIGS absorber [8, 9]. In particular, ZnS exhibits a band gap that can be adjusted according to its composition and deposition condition, ranging from 3.6 to 3.8 eV, as well as a tunable conduction band shift. When properly

controlled, these properties allow for improved charge separation and a significant reduction in recombination at the interface [10, 11]. Several studies have demonstrated that ZnS can significantly enhance device performance when used as a Cd-free buffer layer in CIGS solar cells [4, 7]. Various synthetic routes have been employed for the preparation of II–VI semiconductor alloys. However, solvothermal processes provide important advantages including low-temperature operation, controlled nucleation, uniform particle size distribution, and high chemical purity [12]. Recent advances in solvothermal synthesis allow the fabrication of high-purity nanocrystalline powders that can be used as source materials for sputtering targets [13, 14]. These characteristics make solvothermal synthesis a suitable technique for producing ZnS materials with tailored structural and optical properties for photovoltaic applications [15-18].

In addition to experimental invention, the numerical simulation has become an important tool for understanding in depth and optimizing the performance of heterojunction solar cells. Software such as SCAPS-1D allows thorough analysis of band alignment, interface defects, recombination mechanisms, and device optimization strategies [19, 20]. Combining experimental characterization with numerical modeling offers a deeper understanding of the CIGS/ZnS interface and helps to design high-performance Cd-free device structures. The present work proposes a combined experimental and numerical investigation of ZnS buffer layers prepared from solvothermal technique. After synthesizing ZnS nanopowders, thin films were deposited by rf-magnetron sputtering and we report the structural, morphological, and optical characterization of ZnS thin layer. These data were then implemented in SCAPS-1D simulations to estimate the performance of a CIGS/ZnS solar cell.

In this study, the impact of the thickness of the ZnS and CdS buffer layer on the photovoltaic performance of a CIGS solar cell was systematically investigated. This analysis focused on the current-voltage (*J-V*) characteristics, the external quantum efficiency (*QE*) curves, and the main photovoltaic parameters: open-circuit voltage (V_{oc}), short-circuit current density (J_{sc}), fill factor (*FF*), and the conversion efficiency (η). The main objective was to identify the optimal device configurations [21, 22].

The experimental results show good agreement with the numerical simulation outcomes and are compatible with values described in the literature [23-25]. This consistency between experiment and simulation validates the SCAPS parameters adopted in this study. Nevertheless, as already emphasized, the main objective of this study is to analyze the performance trends and design principles of the device, as well as to establish absolute optimal efficiency values.

2 Experimental details

The ZnS nanowpowders were synthesized via solvothermal method using 99% pure ethylenediamine ($C_2H_8N_2$) as solvent. The precursors were zinc nitrate hexahydrate $Zn(NO_3)_2$-$6H_2O$ and thiourea CH_4N_2S. The reaction was carried out under subcritical conditions in a 1 L autoclave at pressures up to 140 bars and temperatures near 300 °C, with temperature controlled by an external programmable furnace. After the reaction, the obtained product was filtered, rinsed, and dried to yield nanostructured powders.

In the second steps, the powders prepared were pressed into 50 mm diameter targets using a hydraulic press. We deposited ZnS thin films onto glass substrates by rf-magnetron sputtering using nanoparticles synthesized by solvothermal techniques. All samples were prepared at a sputtering power of 40 W. The argon flow rate in the chamber was 20%, with 30% corresponding to 1 L/hour. The distance between the target and the substrate was set at 75 mm. The layer thickness was approximately 300 nm, determined by a piezoelectric balance inserted in the sputtering frame. These deposition conditions were the same for all the thin films prepared.

3 Experimental results and discussion

The X-ray diffraction (XRD) pattern of the ZnS powder prepared by the solvothermal technique is shown in Fig. 1. The powders were treated at 300 °C for one hour in air in a muffle furnace. A comparison of the intensities and positions of the peaks in this pattern with those reported in the JCPDS Card No. 75-1534, Indicates that the ZnS powder consists of hexagonal wurtzite polycrystalline material. The peaks appearing at 2θ values of 26.91°, 28.6°, and 30.54° correspond respectively to the (100), (002), and (101) planes of wurtzite ZnS. Additionally, the peak positions provide lattice parameters of a = 3.82 Å and c = 6.24 Å, characteristic of the P63mc space group symmetry [12]. Using the Scherrer equation, the grain size was estimated to be approximately 18 nm. These results are consistent with those reported by several researchers [26, 27].

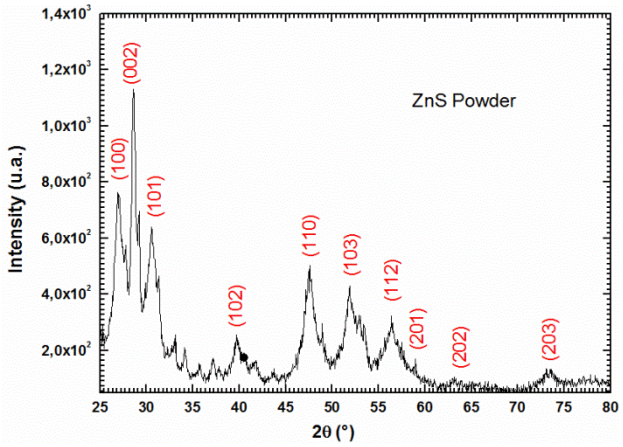


Fig. 1 X-ray diffraction pattern of ZnS powder.

The synthesized materials underwent Energy-dispersive X-ray spectroscopy (EDS) analysis to identify their chemical elements. The atomic percentage measurements for zinc and sulfur in ZnS powders show 55.24% zinc and 44.76% sulfur which matches the expected stoichiometric ratio thus demonstrating both high chemical purity and excellent compositional uniformity. The near-stoichiometric composition indicates that the synthesis method worked well while showing only small amounts of contaminants.

The X-ray diffraction patterns of ZnS thin films prepared through RF magnetron sputtering of solvothermally made nanopowders appear in Fig. 2(a) and b. The XRD analyses of ZnS thin films which were deposited at room temperature and at 200 °C substrate temperature indicate that, the film crystallinity shows better improvement when the sample receives deposition at 200 °C instead of room temperature deposition. The preferred (111) orientation which matches cubic ZnS structures becomes evident in this study.

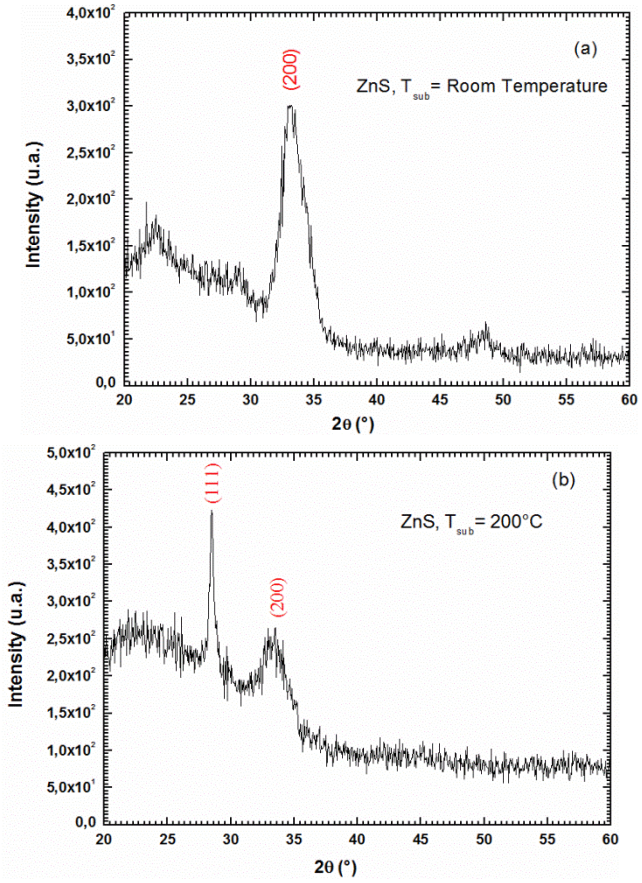


Fig. 2 XRD patterns of ZnS layers grown at substrate temperatures of (a) room temperature and (b) 200 °C.

Furthermore, the obtained result shows that substrate temperature affects both crystallite size and lattice strain of the material. The XRD analysis produced the essential structural parameters which are presented in Table 1.

Table 1 Lattice parameters (a), grain sizes (D), interplanar spacing (d_{hkl}) and full widths at half height (β) of ZnS powder

Material	Temperature of substrate (°C)	Lattice parameters (Å)	D (nm)	d_{hkl} (Å)	B (rad)
ZnS	Room	a= 5.39	4	2.96	0.035
ZnS	200°C	a= 5.42	30	3.13	0.004

The EDS analyses of ZnS thin films at room temperature and 200 °C substrate temperatures are reported in Table 2. The atomic structure of ZnS thin films maintains near-stoichiometric ratios regardless of the nanopowder production technique while the 200 °C deposition temperature yields the most accurate stoichiometric ratios. However, a slight deviation from the ideal stoichiometric ratio is observed. The small discrepancies which appear in nanomaterials stem from surface effects and intrinsic defects and minor changes during the synthesis process [28, 29]. Importantly, the measured value shows no negative impact on powder crystallinity because the solvothermal method produces highly crystalline materials [30, 31]. The solvothermal technique enables researchers to create highly crystalline nanomaterials with specific chemical makeup and structural design which makes it an ideal method for II–VI semiconductor compound synthesis [32, 33].

Table 2 Element composition ratio of ZnS films

Material	Temperature of substrate (°C)	Atomic compositions (%)	
		Zinc	Sulfur
ZnS	Room	56.40	43.60
ZnS	200	51.39	48.61

The ZnS thin films which glass substrates supported underwent atomic force microscopy (AFM) tapping mode analysis to study their surface topography. The resulting films exhibit homogeneous, well-polished surfaces characterized by low roughness, as shown by the values summarized in the table 3 and the corresponding AFM images (Fig. 3a and b). The results show that these films are composed of relatively compact nanometric particles, with dimensions comparable to those of the grains in the ZnS powder used. However, a significant increase in roughness was observed for films made from powders synthesized via solvothermal methods when the substrate temperature reached 200 °C. This increase in roughness was also accompanied by an increase in grain size. Those are evenly spread throughout the surface thus demonstrating excellent film coverage and continuous film structure. The sputtering process created films which show no signs of cracks or pinholes or voids because the films maintain excellent bonding with their substrate material.

Table 3 Surface roughness of ZnS films.

Material	Temperature of substrate (°C)	RMS (nm)
ZnS	Room	1.27
ZnS	200	43.70

The quantitative evaluation of AFM data reveals that the root-mean-square (RMS) surface roughness values stay at a low level which makes these layers suitable for CIGS solar cell buffer applications. The device performance improves when the buffer/absorber junction contains minimal interface defects and recombination centers because smooth surface morphology enables better charge.

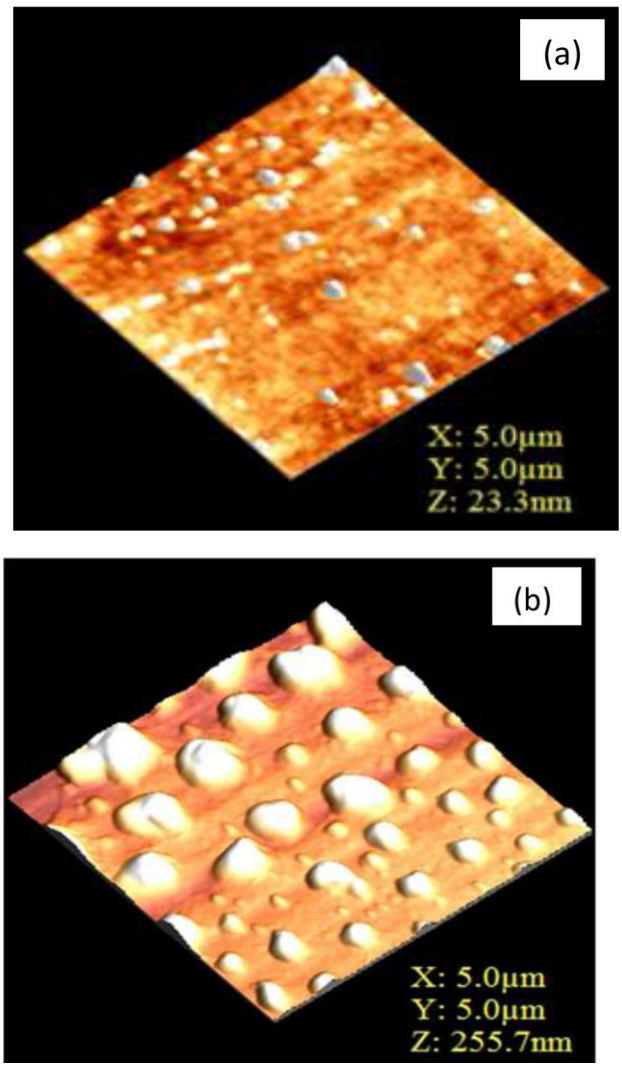


Fig. 3 AFM of ZnS thin films deposited at substrate temperatures of (a): room temperature and (b): 200 °C,

The optical transmission spectra of ZnS thin films deposited by rf-magnetron sputtering from solvothermal powder products appear in Fig. 4. The ZnS thin films show complete optical transparency through the visible spectrum because their spectra reveal 90% average transmittance for each deposited layer. The high level of transparency in this material allows it to transmit most solar spectrum wavelengths [12]. The properties of ZnS thin films make them suitable for buffer layer applications in solar cells because they function as transparent layers. The visible wavelength range shows minimal absorbance at its lowest point. Furthermore, the transmission values decrease rapidly when wavelengths fall below 480 nm because ZnS absorbs light through electronic transitions which occur between its valence and conduction bands. The absorption edge serves as a standard method to calculate the optical bandgap energy. The thin film spectra show interference fringes which result from multiple reflections through the films because the films maintain both uniform thickness and homogeneous structure. The films become more transparent when substrate temperature increases because the deposition process eliminates a volatile substance which produces more uniform films. This result reflects the good morphological quality of the surface.

The absorption coefficient $\alpha(\lambda)$ was calculated from the transmission values, according to the Beer-Lambert equation:

$$\alpha = \frac{1}{d} ln \frac{1}{T} \qquad (1)$$

Where d is the sample thickness and T is the transmission coefficient (%). For allowed an direct transitions [34], which are the case for zinc sulfide, the absorption coefficient α as a function of the photon energy $h\nu$ is expressed as follows:

$$\alpha(h\nu) = A(h\nu - E_g)^{\frac{1}{2}} \qquad (2)$$

Where A is a constant dependent on the material and E_g is the optical band gap energy.
By plotting $(\alpha h\nu)^2$ as a function of $h\nu$, the value of the optical band gap E_g can be determined by extrapolation up to $(\alpha h\nu)^2 = 0$.

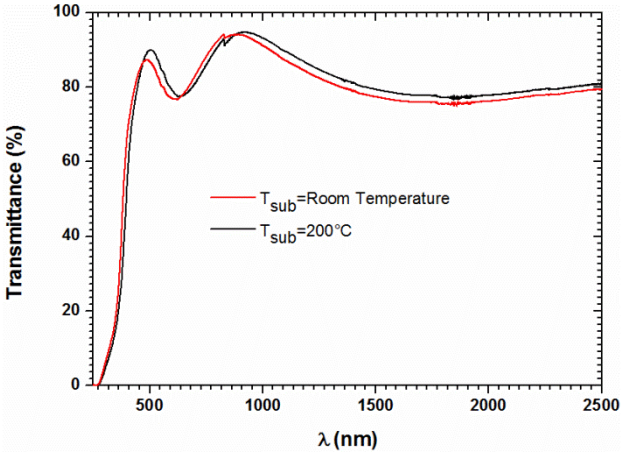


Fig. 4 Transmission spectra of ZnS thin films.

Fig. 5 shows the linear extrapolation of the band-to-band absorption of our layers.
The optical bandgap values obtained for the ZnS layers range from 3.68 to 3.80 eV which matches the values found in previous studies [35, 36]. The bandgap energy shows an increase when we raise the substrate temperature during the process. This corresponds to the band gap increase effect described in the literature [12, 36]. The films undergo structural changes when substrate temperature increases which results in different optical properties. The observed bandgap widening shows a direct relationship with the growing grain size which becomes more significant when the deposition temperature increases. The band gap values in our ZnS layers range from 3.68 to 3.8 eV. These results are consistent with those found by other authors [34-36]. Furthermore, we observed that the band gap energy increases with substrate temperature. This corresponds to the band gap increase effect described in the literature [12, 37]. Increasing the substrate temperature thus leads to a reorganization of the structure. This increase in band gap energy can also be correlated with grain size, which increases with temperature.

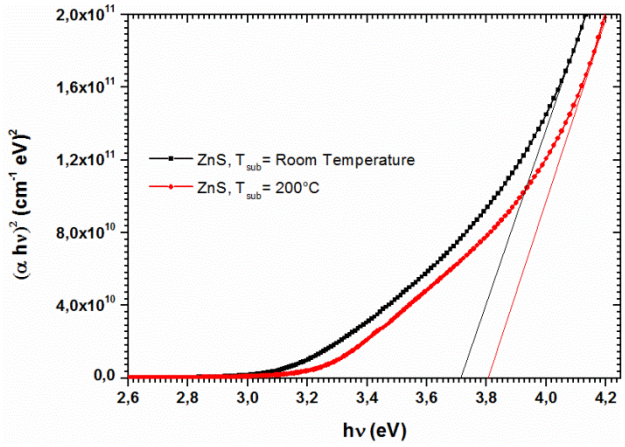


Fig. 5 Variation of $(\alpha h\nu)^2$ as a function of $(h\nu)$ for ZnS thin films obtained at different deposition temperatures.

4 Device structure and simulation

4.1 Modeling tool

In this study, we used the software SCAPS-1D to evaluate the device's performance as the buffer layer's design has varied. The semiconductor device simulation through numerical modeling requires solving the Poisson equation together with electron and hole continuity equations [21, 22, 38]. The SCAPS-1D model solves three differential equations which operate under specific boundary conditions to calculate electrostatic potential and electrons and holes quasi-Fermi levels across the entire device structure [39]. The calculation of these quantities at different depths enables researchers to calculate the (*J-V*) characteristics and the *QE(λ)* curves, and obtain essential photovoltaic parameters which include the V_{oc}, J_{sc}, *FF* and the efficiency η. These standard measurement parameters explain the performance of solar cells [22],

The solar cell structure we have chosen to study and simulate Exhibits a multilayer structure made up of deposited thin films: n-ZnO:Al/i-ZnO/n- ZnS/p-CIGS/Mo/SLG. The TCO layer is necessary to form the front electrode while ensuring the most favorable transmission of the photons of the solar spectrum. In this case ZnO:Al was selected for its exceptional conductivity; therefore, it is a wide-gap material. The thin layer of ZnS is deposited directly onto the CIGS absorber layer, this thin layer is involved in forming the p-n junction, which also ensure the protection the CIGS surface. The typical CIGS solar cell proposed and used for the simulation is illustrated in Fig. 6.

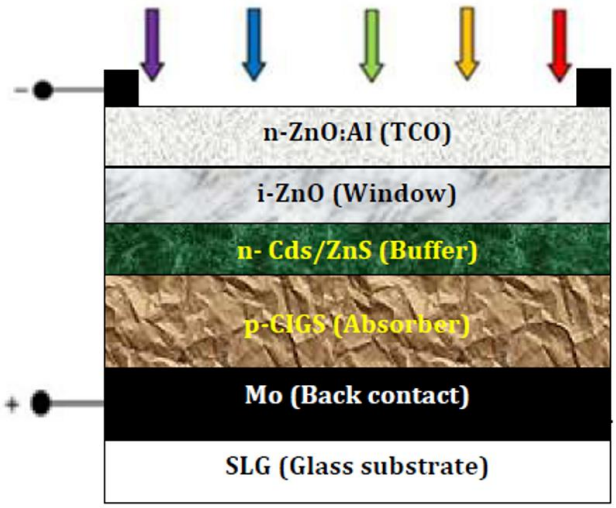


Fig. 6 Device structures of a CIGS thin film solar cell.

The simulations need the input of device parameters, and the interface recombination velocities have been fixed as 10^7 cm/s. The light reflection of the back and the front contacts were assumed to be 0.8 and 0.1, respectively. The AM 1.5D solar radiation was adopted as the illumination source, equivalent to a power of 1000 W/m^2. The measured optical parameters of the ZnS layer from our experimental data were implemented. The material parameters of each semiconductor layer in the simulated cell were given in Table 4. Reported in the scientific literature [21, 40-43].

Table 4 Input parameter used in simulations.

Parameters	**n-ZnO:Al**	**i-ZnO**	**n-CdS**	**n-ZnS**	**p-CIGS**
Layer thickness : d (nm)	250	50	Varied	varied	3000
Dielectric constant : ε_r	9	9	10	10	13.6
Effective conduction band density:N_c (cm^{-3})	$2.2x10^{18}$	$2.2x10^{18}$	$2.2x10^{18}$	$2.2x10^{18}$	$2.2x10^{18}$
Effective valence band density:N_v (cm^{-3})	$1.8x10^{19}$	$1.8x10^{19}$	$1.8x10^{19}$	$1.8x10^{19}$	$1.8x10^{19}$
Doping concentration:(N_a/N_d) (cm^{-3})	$1x10^{19}$	$1x10^{14}$	$1x10^{17}$	$1x10^{16}$	$2x10^{16}$
Band gap: E_g (eV)	3.30	3.30	2.4	3.68	1.20
Electron affinity: χ (eV)	4.45	4.45	4.2	4.35	4.50
Electron mobility: μ_e (cm^2/V.s)	100	100	70	70	50
Hole mobility: μ_h (cm^2/V.s)	25	25	30	30	12
Defect density: N_{DG}/N_{AG} (cm^{-3})	$1.5x10^{14}$	$1.5x10^{14}$	$1.5x10^{17}$	$1.5x10^{17}$	$1x10^{12}$
Capture cross-section electrons: σ_e (cm^2)	$1x10^{-13}$	$1x10^{-13}$	$1x10^{-17}$	$1x10^{-17}$	$1x10^{-13}$
Capture cross-section holes: σ_h (cm^2)	$1x10^{-15}$	$1x10^{-15}$	$1x10^{-12}$	$1x10^{-12}$	$1x10^{-15}$

4.2 Simulation results and discussion

4.2.1 Effect of ZnS and CdS single buffer layer thickness

The study of the influence of the thickness of ZnS and CdS buffer layers on the photovoltaic parameters of the CIGS cell reveals opposing trends between the two materials. For the ZnS layer (Fig. 7a), increasing the thickness from 0.02 µm to 0.10 µm leads to an improvement in efficiency (η), from 22.80% to 22.93%, and in the fill factor (*FF*), which reaches 84.82%. This positive change is linked to better passivation of the interface states and more favorable band alignment. The slight decrease in J_{sc} and V_{oc} remains acceptable, this behavior can be attributed to the wide band gap of ZnS, which effectively minimizes parasitic optical absorption and enhances the transmission of incident photons toward the absorber layer. Conversely, increasing the thickness of the CdS layer (Fig. 7b) causes a systematic degradation of all parameters, the efficiency drops from 24.68% to 22.62%, and the *FF*, J_{sc}, and V_{oc} decrease significantly. This degradation is mainly explained by the significant optical absorption in CdS (gap ≈ 2.4 eV) in the short-wavelength region, as well as by the increase in series resistance and interfacial recombination.

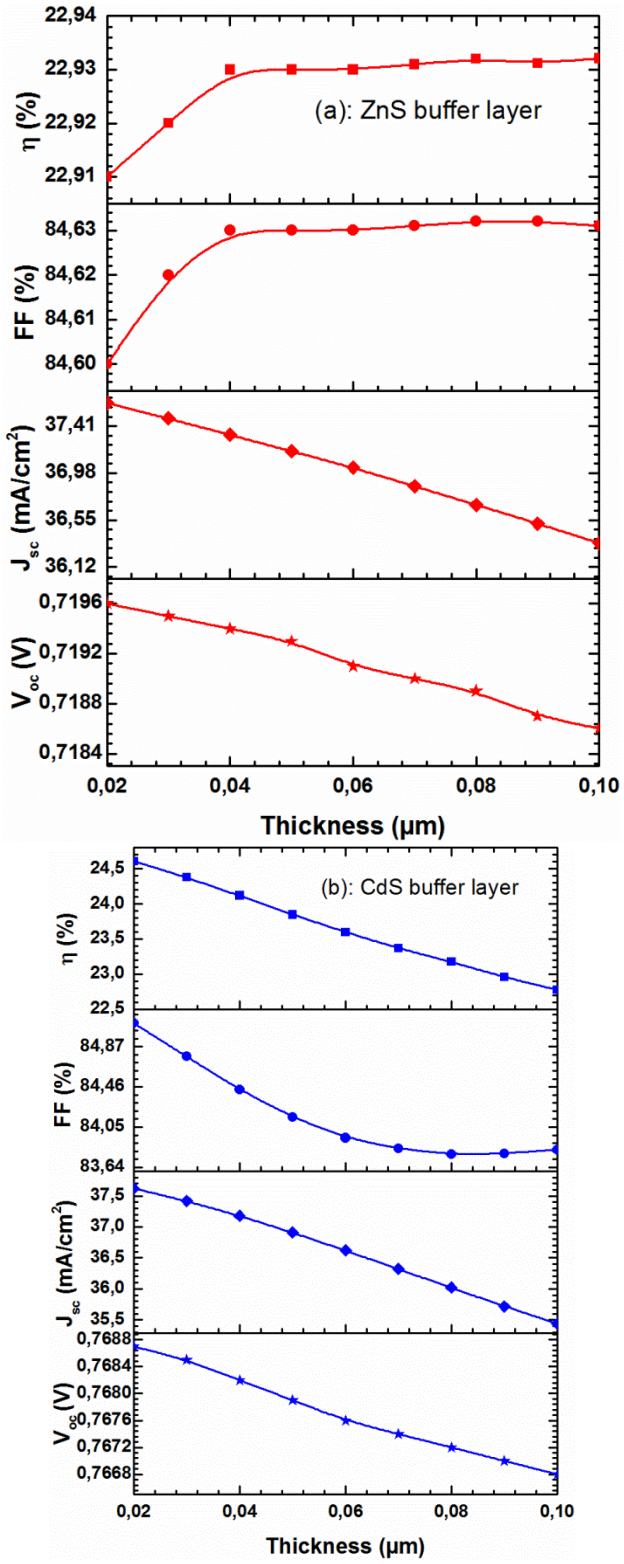


Fig. 7 Calculated dependence of solar cell parameters on ZnS thickness (a) and CdS thickness (b).

The study of the influence of the thickness of the ZnS and CdS buffer layers on the *QE(λ)* reveals distinct behaviors depending on the material. As shown in Fig. 8a and 8b, the *QE* remains high (> 90%) over a wide spectral range from 500 nm to 1100 nm, confirming excellent charge carrier collection and the good optoelectronic quality of the CIGS absorber layer in the visible and near-infrared ranges. However, in the short wavelength region (400–550 nm), an increase in buffer thickness leads to a progressive decrease in *QE(λ)*. This

loss is particularly pronounced in the case of CdS buffer layer, where the thickness increasing from 0.02 µm to 0.1 µm causes a significant drop in quantum efficiency due to its relatively small energy gap (≈ 2.4 eV), resulting in significant parasitic absorption of blue photons. On the other hand, ZnS, with its wider band gap (≈ 3.68 eV), has a less pronounced influence on *QE*, making it an excellent candidate as the first buffer layer in a dual-buffer configuration. These results highlight the importance of optimizing buffer layer thickness: a thin ZnS configuration (0.02–0.04 µm) combined with a very thin CdS (≤ 0.04 µm) maximizes carrier collection across the entire spectrum, thus contributing to the overall improvement of the J_{sc} and the cell efficiency.

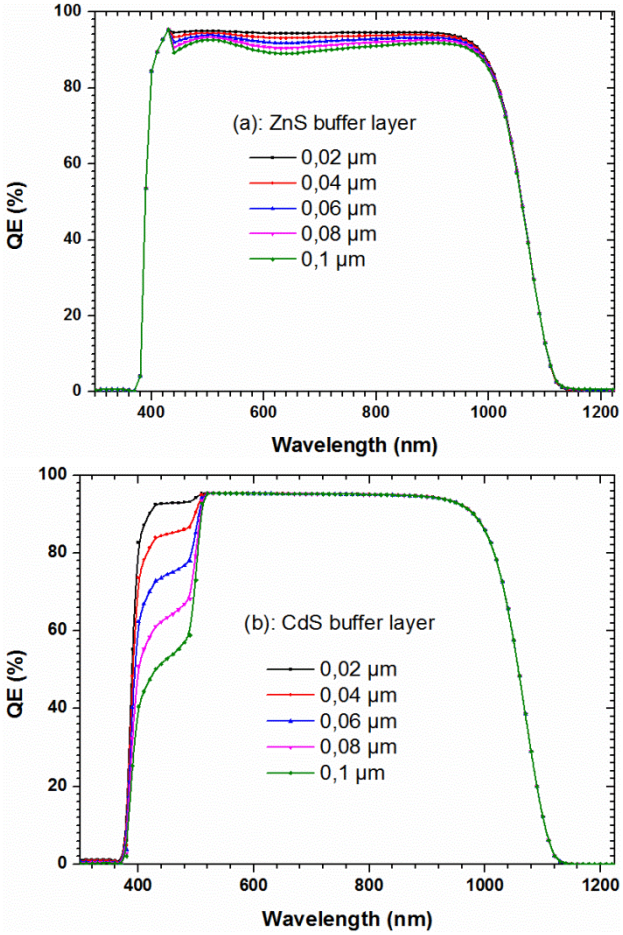
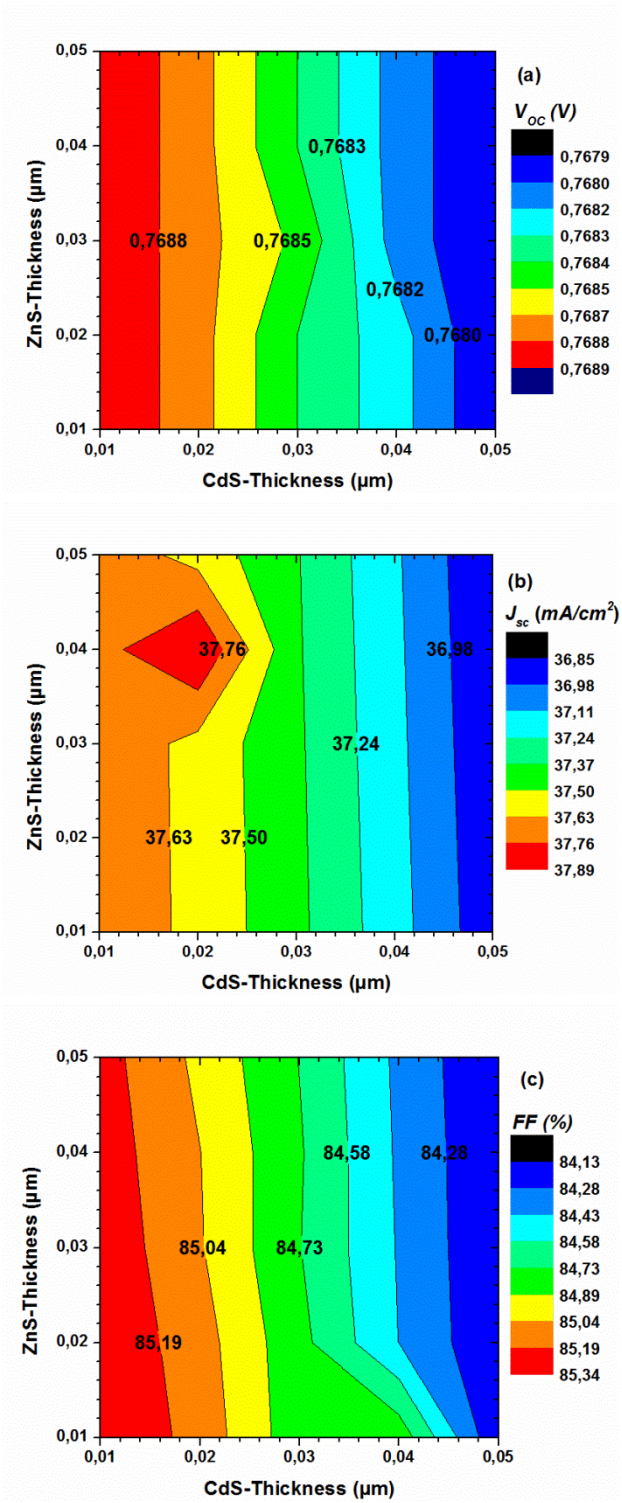


Fig. 8 The dependence of the quantum efficiency on the thickness of ZnS buffer layer (a) and CdS buffer layer (b).

4.2.2 Modeling and performance optimization of bilayer buffer configurations

The analysis of the combined effect of the thickness of the double buffer layer ZnS/CdS on the performance of the CIGS-based solar cell, illustrated by the contour plots in Fig. 9, reveals a strong dependence of the photovoltaic parameters on these thicknesses. The V_{oc} remains relatively stable oscillating between 0.7688 and 0.7703 V as shown in Fig. 9a, indicating good alignment of the bands at the CIGS/ZnS and ZnS/CdS interfaces, enabling effective reduction of surface recombination regardless of the thickness considered within the studied range. In contrast, J_{sc}, *FF*, and especially η show a well-defined optimal range for thin to moderate thicknesses. Regarding the J_{sc}, the results of Fig. 9b show an optimal zone for thin ZnS layers (less than 0.02 µm) and moderate CdS layers (between 0.02 and 0.04 µm), where J_{sc} reaches maximum values close to 38 mA/cm². Beyond these values, a progressive decrease in J_{sc} is observed, mainly attributable to parasitic absorption in the buffer layers, which have wider band gaps than the CIGS, thus reducing the number of photons reaching the absorbing layer. The *FF* follows similar trends indicate by the Fig. 9c, with high values (up to 85.34%) in the thinner layer region. Increasing the thickness of the ZnS and CdS layers leads to a degradation of the *FF*, due to

increased series resistance and a possible increase in defect density at the interfaces. The overall conversion efficiency η, the most critical parameter, has a clearly defined optimal range (Fig. 9d). The maximum efficiency of 24.68% is obtained for a ZnS thickness of approximately 0.01 to 0.02 µm and a CdS thickness of approximately 0.02 to 0.04 µm.



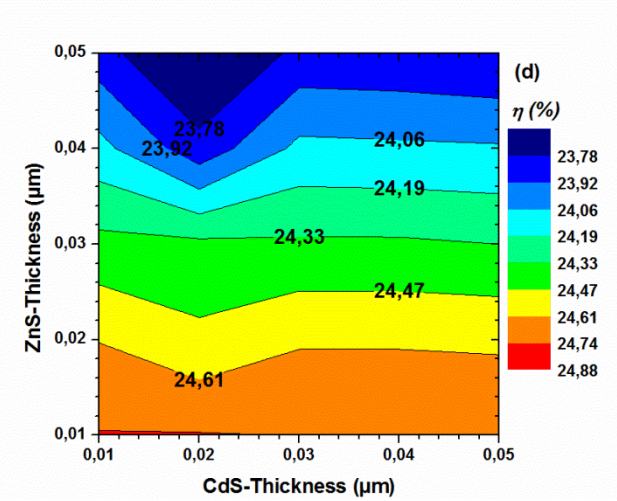


Fig. 9 Effect of ZnS and CdS buffer thickness in double buffer layer on cell performance (a) V_{oc}, (b) J_{sc}, (c) *FF* and (d) η.

This configuration provides an excellent compromise between good interface passivation, high optical transmission, and efficient carrier transport. Beyond these values, increasing the thicknesses leads to a significant decrease in J_{sc} and η, primarily due to parasitic absorption in the buffer layers and an increase in series resistance. These results demonstrate the advantages of the ZnS/CdS dual buffer, which allows for better passivation of the interface and optoelectronic optimization compared to a single buffer, thus opening up promising prospects for the improvement of CIGS cells.

Fig. 10a shows the *J-V* characteristic of the CIGS solar cell with CdS, ZnS, and CdS/ZnS buffer layers. The results show that the performance of the CIGS cell is strongly influenced by the nature of the buffer layer. The cell equipped solely with ZnS exhibits a relatively high J_{sc} due to the high optical transparency of this material, resulting from the wide band gap. However, this structure is characterized by a lower V_{oc}, suggesting a less favorable interface quality and an increase in recombination phenomena at the ZnS/CIGS heterojunction. While the cell using a CdS buffer layer exhibits a significant improvement in V_{oc}. This improvement is primarily attributed to the good energy alignment between the CdS and the CIGS absorber, which promotes the separation and transport of photogenerated carriers while limiting interfacial recombination. However, the relatively narrow band gap of the CdS results in some parasitic absorption of incident radiation in the short-wavelength range, which can slightly limit the generated current. The CdS/ZnS double-buffer structure combines the advantages of both materials, leading to the best values of the *Voc* and the *Jsc*. The CdS/ZnS double layer provides the best overall *J-V* characteristics, while ZnS alone is slightly inferior.

Fig. 10b presents *QE* of CIGS cells incorporating the different buffer layers. The curves show a strong dependence of the spectral response on the nature of the material used as the buffer layer, particularly in the short-wavelength region. The response intensity of the solar cell with ZnS and the CdS/ZnS dual buffer layer is higher than that of the cell with CdS in the short-wavelength band (300 to 380 nm), which explains their higher J_{sc}. In the 450 to 520 nm band, the solar cell with the CdS/ZnS dual buffer layer exhibits higher response intensity than the other configuration, offers the best overall spectral response, reflecting better collection of photogenerated carriers and improved photovoltaic performance of the CIGS cell. In the long-wavelength band, the response of the solar cell with the CdS buffer layer is more pronounced than that of the other cells. The main advantage of the double buffer is the reduction of recombination at the interface while improving absorption in the short wavelength range, which is consistent with the objective of developing Cd-free or low cadmium CIGS cells.

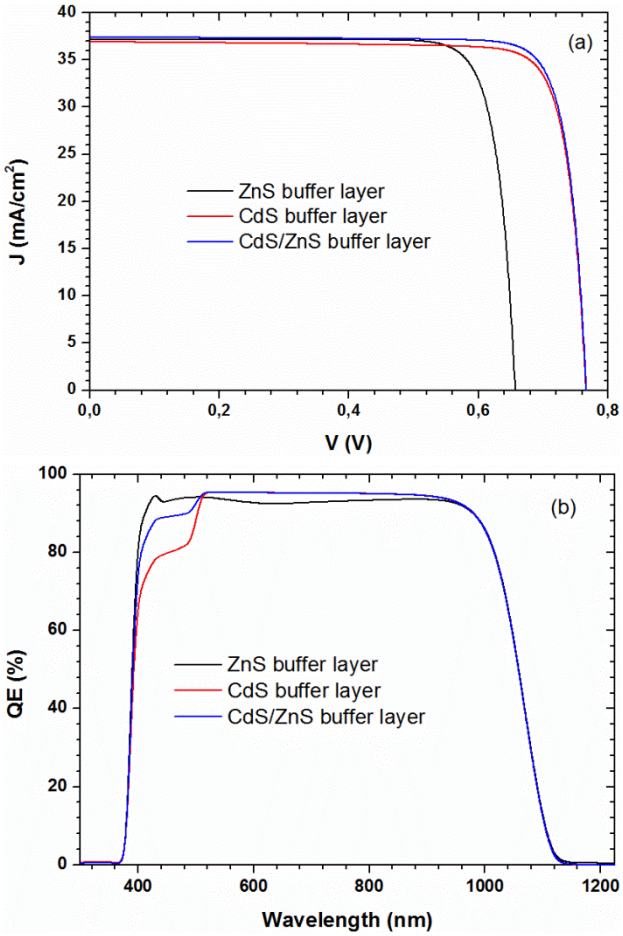


Fig. 10 The *J–V* characteristics (a) and *QE* curve (b) of CIGS cells with CdS, ZnS and CdS/ZnS buffer layers.

5 Conclusions

In this study, the ZnS nanopowders prepared by solvothermal synthesis were successfully used to deposit high-quality ZnS thin films using rf-magnetron sputtering. Structural and optical analyses show that, the ZnS thin films combine high transparency with favorable microstructure, while the thin films produced offer balanced band gap values, suitable for integration into the devices. On the other hand, the simulation study were performed with SCAPS-1D software, the performance of the CIGS solar cells was evaluated using different buffer layers (CdS and ZnS). The results show that the buffer layer thickness strongly influences the main photovoltaic parameters. Although the ZnS buffer layer exhibits a better response in the short-wavelength range compared to CdS, it offers a lower fill factor. To optimize overall performance, a dual-layer CdS/ZnS buffer structure was proposed. This configuration combines the advantages of both materials and improves cell efficiency. These results confirm the superiority of a dual-buffer ZnS/CdS architecture, where a thin ZnS layer (0.02-0.05 µm) acts as both an optical window and a passivation layer, while the CdS layer must be kept very thin (≤ 0.04 µm) to minimize losses. This configuration achieves an excellent compromise between interface passivation and optical transmission, thus representing a promising avenue for optimizing the CIGS solar cells device.

Acknowledgements

Authors' acknowledgments are dedicated to Mr. Marc Burgelman for assuring the availability of SCAPS-1D software.

Author contributions A. Mouhoub: Conceptualization, Methodology, Investigation, Writing–Original Draft, Data processing. W. Chatta: Supervision, Writing–Review & Editing. M. Birane: Investigation, Data curation, Resources, Visualization.

Funding The authors have not disclosed any funding.

Data availability No datasets were generated or analysed during the current study.

Declarations

Conflict of Interest

The authors declare that they have no known competing financial interests or personal relationships that could have appeared to influence the work reported in this paper.

Reference

1. M.A. Green, Y. Hishikawa, E.D. Dunlop, D.H. Levi, J. Hohl-Ebinger, M. Yoshita, A.W.Y. Ho-Baillie, Solar cell efficiency tables (Version 53). Prog. Photovolt. Res. Appl. 27, 3–12 (2019). https://doi.org/10.1002/pip.3102
2. M. Ni, J.M. Liu, Z.Q. Li, Q. Shen, Y.Z. Feng, X.D. Feng, Simulation of graded bandgap on backwall superstrate CIGS solar cells with MoOx electron reflection layer. Mater. Res. Express 6, 116441 (2019). https://doi.org/10.1088/2053-1591/ab4c5c
3. A. Mavlonov, J. Chantana, T. Nishimura, Y. Kawano, M. Inoue, N. Hamada, T. Masuda, T. Minemoto, Superstrate-type flexible and bifacial Cu(In,Ga)Se_2 thin-film solar cells with $In2O_3$:SnO_2 back contact. Sol. Energy 211, 725–731 (2020). https://doi.org/10.1016/j.solener.2020.10.019
4. M.M. Islam, S. Ishizuka, A. Yamada, K. Sakurai, S. Niki, T. Sakurai, K. Akimoto, CIGS solar cell with MBE-grown ZnS buffer layer. Sol. Energy Mater. Sol. Cells 93, 970–972 (2009). https://doi.org/10.1016/j.solmat.2008.11.047
5. A.L. Donne, D. Cavalcoli, R.A. Mereu, M. Perani, L. Pagani, M. Acciarri, S. Binetti, Study of the physical properties of ZnS thin films deposited by RF sputtering. Mater. Sci. Semicond. Process. 71, 7–11 (2017). https://doi.org/10.1016/j.mssp.2017.06.042
6. C. Wang, J. Li, W. Feng, Y. Ye, H. Guo, Effect of seed layer on structure and luminescence properties of ZnS nanostructures. Optik 242, 167095 (2021). https://doi.org/10.1016/j.ijleo.2021.167095
7. X.S. Fang, T.Y. Zhai, U.K. Gautam, L. Li, ZnS nanostructures: From synthesis to applications. Prog. Mater. Sci. 56, 175–287 (2011). https://doi.org/10.1016/j.pmatsci.2010.10.001
8. D. Suthar, G. Chasta, Himanshu, S.L. Patel, S. Chander, M.D. Kannan, M.S. Dhaka, Impact of different annealing conditions on physical properties of ZnSe thin films for ecofriendly buffer layer applications. Mater. Res. Bull. 132, 110982 (2020). https://doi.org/10.1016/j.materresbull.2020.110982
9. M. Wang, G. Fei, Y. Zhang, M. Kong, L. Zhang, Tunable and predetermined bandgap emissions in alloyed ZnS_xSe_{1-x} nanowires. Adv. Mater. 19, 4491–4494 (2007). https://doi.org/10.1002/adma.200602919
10. J. Lu, H. Liu, C. Sun, M. Zheng, M. Nripan, G.S. Chen, G.M. Subodh, X. Zhang, C.H. Sow, Optical and electrical applications of ZnS_xSe_{1-x} nanowire network with uniform and controllable stoichiometry. Nanoscale 4, 976–981 (2012). https://doi.org/10.1039/C2NR11459C
11. D. Wu, Y. Chang, Z. Lou, T. Xu, J. Xu, Z. Shi, Y. Tian, X. Li, Controllable synthesis of ternary ZnS_xSe_{1-x} nanowires with tunable band-gaps for optoelectronic applications. J. Alloys Compd. 708, 623–627 (2017). https://doi.org/10.1016/j.jallcom.2017.03.012
12. R. Mendil, Z. Ben Ayadi, J. Ben Belgacem, et al., The properties of ZnS thin films prepared by rf-magnetron sputtering from nanoparticles synthesized by solvothermal/hydrothermal route. J. Mater. Sci. Mater. Electron. 27, 444–451 (2016). https://doi.org/10.1007/s10854-015-3772-y
13. R. Mendil, Z. Ben Ayadi, K. Djessas, Effect of solvent medium on the structural, morphological and optical properties of ZnS nanoparticles synthesized by solvothermal route. J. Alloys Compd. 678, 87–92

(2016). https://doi.org/10.1016/j.jallcom.2016.03.171
14. R. Mendil, Z.B. Ayadi, C. Vázquez-Vázquez, et al., A new procedure to synthesis of $ZnS_{1-x}Se_x$ nanoparticles by a facile solvothermal method. J. Mater. Sci. Mater. Electron. 29, 10656–10662 (2018). https://doi.org/10.1007/s10854-018-9129-6
15. D.D. Hile, H.C. Swart, S.V. Motloung, T.E. Motaung, I. Ahemen, P.R. Jubu, K.E. Essien, L.F. Koao, Investigating the effects of varying sulfur concentration on ZnS_xSe_{1-x} ($0 \leq x \leq 1.0$) thin films prepared by photo-assisted chemical bath method. Results Opt. 14, 100613 (2024). https://doi.org/10.1016/j.rio.2024.100613
16. J. Liu, A.X. Wei, M.X. Zhuang, Y. Zhao, Investigation of the ZnS_xSe_{1-x} thin films prepared by chemical bath deposition. J. Mater. Sci. Mater. Electron. 24, 1348–1353 (2013). https://doi.org/10.1007/s10854-012-0932-1
17. N.M. Patil, S.G. Nilange, A.A. Yadav, Growth and characterization of ZnS_xSe_{1-x} thin films deposited by spray pyrolysis. Thin Solid Films 664, 19–26 (2018). https://doi.org/10.1016/j.tsf.2018.08.018
18. R.G. Valeev, E.A. Romanov, V.L. Vorobiev, V.V. Mukhgalin, V.V. Kriventsov, A.I. Chukavin, B.V. Robouch, Structure and properties of ZnSxSe1−x thin films deposited by thermal evaporation of ZnS and ZnSe powder mixtures. Mater. Res. Express 2, 025006 (2015). https://doi.org/10.1088/2053-1591/2/2/025006
19. M.S. Uddin, R. Hosen, S. Sikder, H. Mamur, M.R.A. Bhuiyan, Photovoltaic performance enhancement of Al/ZnO:Al/i-ZnO/CdS/CIGS/Pt solar cell using SCAPS-1D software. Next Energy 2, 100080 (2024). https://doi.org/10.1016/j.nxener.2023.100080
20. A. Kakade, K.B. Chavan, S. Chaure, N.B. Chaure, The role of window layers on the simulated performance of CIGS solar cell characteristics using SCAPS-1D. Next Res. 2, 100334 (2025). https://doi.org/10.1016/j.nexres.2025.100334
21. A. Mouhoub, A. Bouloufa, K. Djessas, A. Messous, Device modeling approach and simulation of the effect of the ODC thin layer on bifacial solar cells based on $CuIn_{1-x}Ga_xSe_2$ thin films absorbers. J. Phys. Chem. Solids 144, 109520 (2020). https://doi.org/10.1016/j.jpcs.2020.109520
22. A. Mouhoub, A. Bouloufa, K. Djessas, A. Messous, Analytical modeling and optimization of original bifacial solar cells based on $Cu(In,Ga)Se_2$ thin films absorbers. Superlattices Microstruct. 122, 434–443 (2018). https://doi.org/10.1016/j.spmi.2018.06.068
23. S. Ray, B. Barman, C. Darshan, K. Tarafder, K.V. Bangera, ZnS_xSe_{1-x} thin films: A study into its tunable energy band gap property using an experimental and theoretical approach. Sol. Energy 240, 140–146 (2022). https://doi.org/10.1016/j.solener.2022.05.019
24. H.K. Sadekar, A.V. Ghule, R. Sharma, Bandgap engineering by substitution of S by Se in nanostructured $ZnS_{1-x}Se_x$ thin films grown by soft chemical route for nontoxic optoelectronic device applications. J. Alloys Compd. 509, 5525–5531 (2011). https://doi.org/10.1016/j.jallcom.2011.02.089
25. B. Abdallah, M. Kakhia, N. Alkafri, Investigation of ZnS nanotubes films: Morphological, structural and optical properties. J. Nano Res. 60, 142–153 (2019). https://doi.org/10.4028/www.scientific.net/J.NanoR.60.142
26. J. Madhavi, V. Prasad, ZnS and ZnS/CdS core-shell nanoparticles: Synthesis, properties and perspectives. Surf. Interfaces 21, 100757 (2020). https://doi.org/10.1016/j.surfin.2020.100757
27. B. Kaur, K. Singh, A.K. Malik, Effect of ligands on crystallography, morphology and photocatalytic ability of ZnS nanostructures. Dyes Pigm. 142, 153–160 (2017). https://doi.org/10.1016/j.dyepig.2017.03.013
28. J. Zhou, J. Zhao, R. Liu, Defect engineering of zeolite imidazole framework derived ZnS nanosheets towards enhanced visible light driven photocatalytic hydrogen production. Appl. Catal. B Environ. 278, 119265 (2020). https://doi.org/10.1016/j.apcatb.2020.119265
29. B. Belache, Y. Khelfaoui, M. Bououdina, T. Souier, W. Cai, Structural and optical properties of silica single-layer films doped with ZnS quantum dots: Photoluminescence monitoring of annealing-induced defects. Mater. Sci. Semicond. Process. 76, 42–49 (2018). https://doi.org/10.1016/j.mssp.2017.12.013
30. X. Liu, X. Zhang, Y. Liu, M. Liu, X. Miao, Y. Wang, Influence of ZnS crystal morphology on adsorption-photocatalytic efficiency of pseudocrystal ZnS nanomaterials for methylene blue degradation. J. Mol. Struct. 1256, 132514 (2022). https://doi.org/10.1016/j.molstruc.2022.132514
31. Z. Yin, M. Li, N. Wang, Z. Zhou, Y. Hu, D. Fan, Y. Pang, Y. Liu, Z. Lu, J. Hai, Deposition of CdS and

ZnS directly on rGO via an emulsion-solvothermal method for excellent photocatalytic activity and stability. Appl. Surf. Sci. 612, 155844 (2023). https://doi.org/10.1016/j.apsusc.2022.155844

32. W. Gao, M. Cao, W. Xiao, F. Lei, J. Huang, Y. Sun, L. Wang, Y. Shen, Effects of reaction conditions on the structural, morphological and optical properties of solvothermal synthesized ZnS nanostructures. Mater. Sci. Semicond. Process. 56, 349–356 (2016). https://doi.org/10.1016/j.mssp.2016.09.020
33. L. Chai, W. He, L. Sun, F. Jin, X. Hu, J. Ma, Solvothermal synthesis of wurtzite ZnS complex spheres with high hierarchy. Mater. Lett. 120, 26–29 (2014). https://doi.org/10.1016/j.matlet.2014.01.028
34. P.K. Ghosh, S. Jana, S. Nandy, K.K. Chattopadhyay, Size-dependent optical and dielectric properties of nanocrystalline ZnS thin films synthesized via rf-magnetron sputtering technique. Mater. Res. Bull. 42, 505–514 (2007). https://doi.org/10.1016/j.materresbull.2006.06.019
35. M. Ambrico, V. Stagno, D. Smaldone, R. Martino, G. Perna, V. Capozzi, Pulsed laser deposition of ZnS_xSe_{1-x} and CdS_xSe_{1-x} thin films on quartz: Measurements of energy gap, absorption coefficient, and refractive index. Proc. SPIE 3404, 39–46 (1998). https://doi.org/10.1117/12.308654
36. K.T. Ramakrishna Reddy, Y.V. Subbaiah, T.B.S. Reddy, D. Johnston, I. Forbes, R.W. Miles, Pyrolytic spray deposition of ZnS_xSe_{1-x} layers for photovoltaic applications. Thin Solid Films 431, 340–343 (2003). https://doi.org/10.1016/S0040-6090(03)00154-8
37. M.A. Iqbal, S. Bakhsh, S.S. Maidin, K. Morsy, J.R. Choi, A.C. Alguno, Investigating structural and optoelectronic properties of Cr-substituted ZnSe semiconductors. Sci. Rep. 14, 15510 (2024). https://doi.org/10.1038/s41598-024-66378-2
38. T. Chargui, F. Lmai, K. Rahmani, Advancements in CIGS/ZnS heterojunction solar cells: Experimental and numerical analysis. Optik 314, 172008 (2024). https://doi.org/10.1016/j.ijleo.2024.172008
39. S. Mazumder, K. Senthilkumar, Device study and optimisation of CZTS/ZnS based solar cell with CuI hole transport layer for different conduction band offset. Sol. Energy 237, 414–431 (2022). https://doi.org/10.1016/j.solener.2022.03.036
40. S. Tobbeche, S. Kalache, M. Elbar, Improvement of the CIGS solar cell performance: Structure based on a ZnS buffer layer. Opt. Quantum Electron. 51, 284 (2019). https://doi.org/10.1007/s11082-019-2000-z
41. S. Singh, T. Yadav, A. Sahu, Performance enhancement of CIGS/CZTS-based thin film solar cell using non-toxic ZnS buffer layer: A simulation approach. J. Opt. 53, 4050–4058 (2024). https://doi.org/10.1007/s12596-023-01589-w
42. P. Xin, J.K. Larsen, F. Deng, W.N. Shafarman, Development of $Cu(In,Ga)Se_2$ superstrate devices with alternative buffer layers. Sol. Energy Mater. Sol. Cells 157, 85–92 (2016). https://doi.org/10.1016/j.solmat.2016.05.018
43. D.H. Hwang, J.H. Ahn, K.N. Hui, K.S. Hui, Y.G. Son, Structural and optical properties of ZnS thin films deposited by RF magnetron sputtering. Nanoscale Res. Lett. 7, 26 (2012). https://doi.org/10.1186/1556-276X-7-26